Hu et al. *NPG Asia Materials* (2021) 13:35
https://doi.org/10.1038/s41427-021-00304-0

NPG Asia Materials

ARTICLE Open Access

Matrix stiffness changes affect astrocyte phenotype in an in vitro injury model

Yan Hu[1,2], Guoyou Huang[1,2,3], Jin Tian[1,2], Jinbin Qiu[1,2], Yuanbo Jia[1,2], Dayun Feng[4], Zhao Wei[1,2], Sidi Li[5] and Feng Xu[1,2]

Abstract

Injury to the central nervous system (CNS) usually leads to the activation of astrocytes, followed by glial scar formation. The formation of glial scars from active astrocytes in vivo has been found to be dependent on the cell microenvironment. However, how astrocytes respond to different microenvironmental cues during scar formation, such as changes in matrix stiffness, remains elusive. In this work, we established an in vitro model to assess the responses of astrocytes to matrix stiffness changes that may be related to pathophysiology. The investigated hydrogel backbones are composed of collagen type I and alginate. The stiffness of these hybrid hydrogels can be dynamically changed by association or dissociation of alginate chains through adding crosslinkers of calcium chloride or a decrosslinker of sodium citrate, respectively. We found that astrocytes obtain different phenotypes when cultured in hydrogels of different stiffnesses. The obtained phenotypes can be switched in situ when changing matrix stiffness in the presence of cells. Specifically, matrix stiffening reverts astrogliosis, whereas matrix softening initiates astrocytic activation in 3D. Moreover, the effect of matrix stiffness on astrocytic activation is mediated by Yes-associated protein (YAP), where YAP inhibition enhances the upregulation of GFAP and contributes to astrogliosis. To investigate the underlying mechanism of matrix stiffness-dependent GFAP expression, we also developed a mathematical model to describe the time-dependent dynamics of biomolecules involved in the matrix stiffness mechanotransduction process of astrocytes. The modeling results further indicate that the effect of matrix stiffness on cell fate and behavior may be related to changes in the cytoskeleton and subsequent activity of YAP. The results from this study will guide researchers to re-examine the role of matrix stiffness in reactive astrogliosis in vivo and inspire the development of a novel therapeutic approach for controlling glial scar formation following injury, enabling axonal regrowth and improving functional recovery by exploiting the benefits of mechanobiology studies.

Introduction

Injury to the central nervous system (CNS) usually induces astrocytic reactivity, followed by glial scar formation[1]. For years, glial scarring has been thought to be a major obstacle to successful axon regeneration[2,3]. However, recently accumulated evidence suggests a beneficial role for this scar tissue as part of the endogenous local immune regulation and repair process[1,4,5]. At an early stage after injury, the glial scar protects damaged neural tissue by preventing an overwhelming inflammatory response and reestablishing the blood–brain barrier[6–8]. On the other hand, at later stages, scarred tissue releases biochemical factors (e.g., chondroitin, heparan, dermatan, and keratan sulfate proteoglycans[8]), which may impair axonal outgrowth, causing aberrant function or death of neurons[6–8]. As a result, it is crucial to regulate the formation of glial scars during treatment of neural injury.

Moreover, as the key effector cells in glial scar formation, astrocytes have been found to change their phenotype from naive astrocytes to reactive astrocytes and

Correspondence: Feng Xu (fengxu@mail.xjtu.edu.cn)
[1]The Key Laboratory of Biomedical Information Engineering of Ministry of Education, Xi'an Jiaotong University, Xi'an 710049, P.R. China
[2]Bioinspired Engineering and Biomechanics Center (BEBC), Xi'an Jiaotong University, Xi'an 710049, P.R. China
Full list of author information is available at the end of the article
These authors contributed equally: Yan Hu, Guoyou Huang

gradually into scar-forming astrocytes, upregulating glial fibrillary acidic protein (GFAP)[9–11] and vimentin[12] and inflammatory proteins such as IL-1β[13]. Such astrocytic phenotype transformation has been found to depend on the cell microenvironment in vivo[14]. For example, reactive astrocytes could revert in retrograde to naive astrocytes in a proper microenvironment. The phenotypic changes of astrocytes are affected by multiple microenvironmental cues, one of which is matrix stiffness[15–18]. Glial scars in both the rat cortex and spinal cord are significantly softer than those in healthy CNS tissues[6]. Several in vitro models have been developed to study the influences of matrix stiffness on astrocyte phenotypic changes[15–18]. For example, by culturing astrocytes on substrates of different stiffnesses, it was found that a stiff substrate induces the activation of astrocytes[15–17]. However, the influences of dynamic changes in matrix stiffness on astrocyte behaviors have not been reported, although matrix stiffness usually changes dynamically during glial scar formation. Recently, the phenotype of astrocytes plated on reversible fibrous supramolecular hydrogel was found to be capable of switching reversibly, where the reversible hydrogel can undergo reversible formation and disappearance of superstructures[18]. However, the relationship between astrocyte phenotypic switching and hydrogel stiffness changes remains elusive since the mechanical and structural changes of the hydrogel are not decoupled. Moreover, the above studies were established in 2D culture[14–16,18–21], which failed to recapitulate the native 3D cell microenvironment. Therefore, it is still of great interest to study the effects of dynamic changes in matrix stiffness on astrocyte phenotypic switching in 3D culture.

In this work, we established an in vitro model to study the effects of dynamically changing matrix stiffness on astrocyte phenotypic switching in 3D, which is related to the glial scar-forming process. The hybrid hydrogels were composed of collagen type I, a representative matrix under pathological conditions, and alginate, an inherently bioinert material that was introduced to dynamically tune the mechanical properties of the hydrogel. The responses of astrocytes to different matrix stiffnesses were evaluated by characterizing the expression of GFAP and interleukin 1 beta (IL-1β). The stiffness of the hybrid hydrogels was further tuned in situ to investigate the effects of matrix stiffening and softening on astrocyte phenotypic switching. We found that astrocytes develop an activated phenotype in soft hydrogels but maintain an inactive phenotype in stiff hydrogels. Stiffening soft hydrogels reverts the activation of astrocytes, whereas softening the stiff matrix induces astrocyte activation. Yes-associated protein (YAP) was found to be involved in matrix stiffness-mediated astrocyte activation. We also developed a mathematical model to study the underlying mechanism of matrix stiffness-dependent GFAP expression, and the modeling results were consistent with the experimental results. Based on the mathematical model, we further speculate that the effect of matrix stiffness on cell fate and behavior may be related to changes in the cytoskeleton and the subsequent activity of YAP. These results may improve the understanding of astrocyte mechanobiology and inspire the development of novel therapeutic approaches for treating CNS injury.

Results

Matrix stiffness regulates astrocyte activation in 3D

Recent studies have proven that the stiffness of glial scars is significantly lower than that of healthy neural tissue, which is associated with increased concentrations of softer extracellular matrix (ECM) components[6] (e.g., CSPGs[22] and GAGs[23]). The elastic stiffness of the cortex can change from ~1 kPa (healthy tissue) to nearly ~50 Pa (scar region)[6]. To mimic the dynamic change in the native cell mechanical microenvironment, we fabricated a set of hybrid hydrogel systems composed of collagen type I and alginate with dynamically tunable stiffness. Collagen type I, the major component of hybrid hydrogels, has been highlighted in many studies for its advantageous features in supporting cell adhesion, growth, and migration[24–27]. Recent studies also proved that the proportion of collagen in the ECM significantly increases after brain injury, which contributes to the scar formation process[6,8,14,18]. Moreover, rat primary astrocytes cultured in proper concentrations of collagen type I can maintain a relatively naive phenotype compared to those of those cultured in 2D[28–30]. The addition of alginate supports cells in a round or spreading state with the same matrix stiffness due to its nonadhesive and nanoporous structures. The most attractive characteristic of alginate hydrogels is that alginate can be crosslinked or decrosslinked reversibly to dynamically tune the mechanical properties of the hydrogel[27,31]. In this work, the stiffness of the hybrid hydrogels was dynamically tuned by crosslinking or decrosslinking alginate with calcium chloride or sodium citrate, respectively (Fig. 1a). According to rheological measurements, the storage moduli of the hybrid hydrogels were found to be tuned from ~42.7 ± 6.3 Pa (soft) to ~990.6 ± 189.3 Pa (stiff) (Fig. 1a), which strongly matches the native situations[6]. We measured the softened and stiffened hydrogels with a rheometer at the same time (Supplementary Fig. 1c). We also applied a custom-designed magnetic tweezer to define the mechanical properties of the inner hydrogels and found that the stiffness was consistent with the rheological results (Supplementary Fig. 1d). By analyzing the swelling performance of the hybrid hydrogels, we found that the swelling ratio of the hybrid hydrogels increased with the addition of increasing concentrations of Ca^{2+} (Supplementary Fig. 1a). Moreover, we evaluated the internal microstructure of the hybrid hydrogels by scanning electron

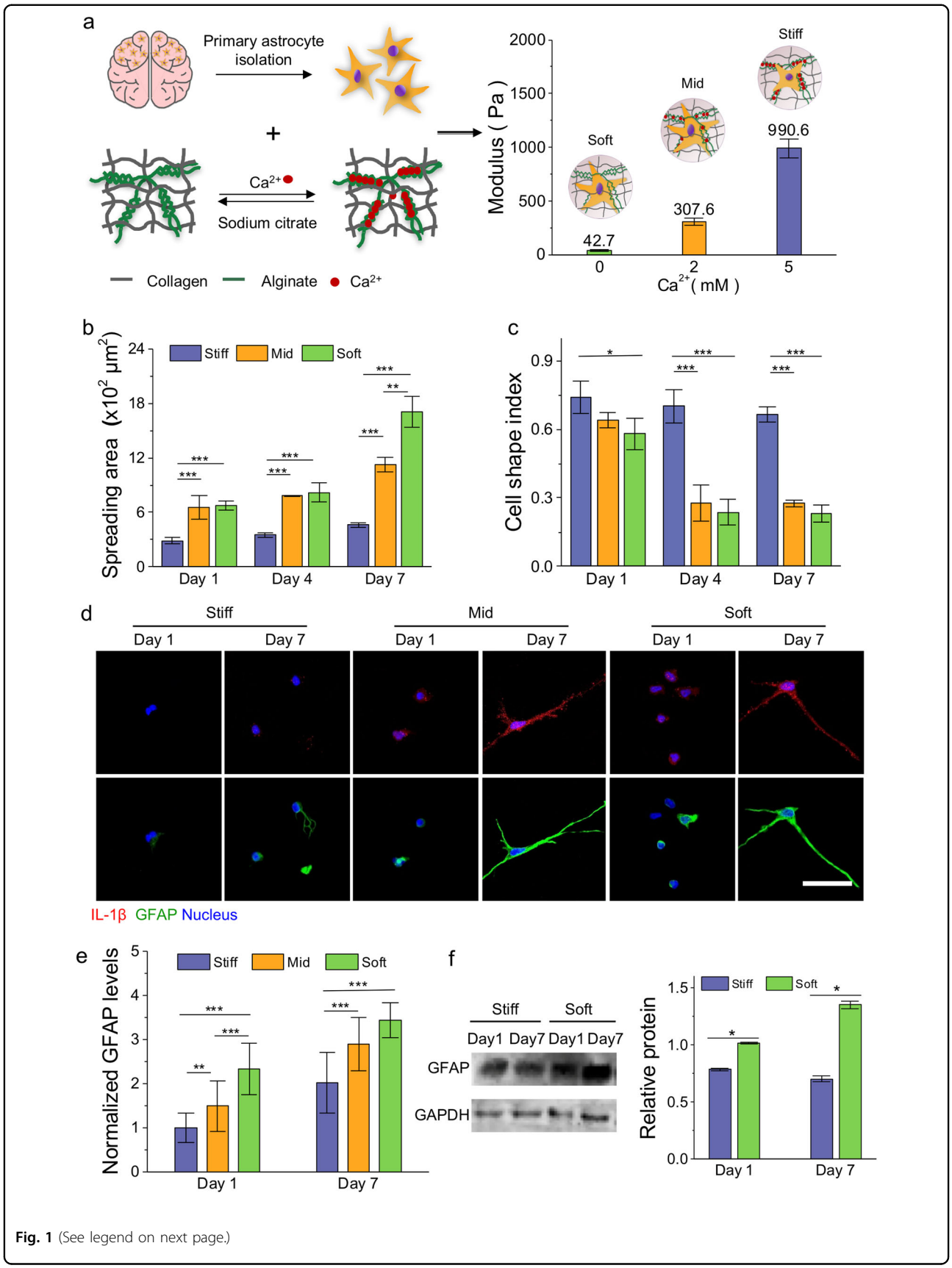

Fig. 1 (See legend on next page.)

(see figure on previous page)
Fig. 1 Matrix stiffness influenced the spreading and activity of astrocytes in 3D. a Astrocytes were encapsulated into hybrid hydrogels of different stiffnesses. The mechanical properties of the hybrid hydrogel changed from ~42.7 ± 6.3 Pa (soft) to ~990.6 ± 189.3 Pa (stiff) when the concentration of Ca^{2+} increased from 0 to 5 mM. **b** The cell spreading area significantly increased with decreasing matrix stiffness. **c** Matrix stiffness influenced the shape of astrocytes. **d**, **e** Immunofluorescence analysis indicated that astrocytes showed increased activity in a softer matrix with upregulated GFAP and IL-1β after 7 days of culture (red, IL-1β; green, GFAP; blue, nucleus). Scale bar, 50 μm. **f** Relative protein levels of GFAP in astrocytes determined by Western blotting. $n > 50$ cells for (**b–e**).

microscopy (SEM) and found that alginate acts as a filler between collagen fibers (Supplementary Fig. 1b).

To assess the biocompatibility of the hybrid hydrogels for culturing astrocytes in 3D, primary astrocytes were isolated from the cortex of neonatal rats, expanded in vitro, and encapsulated into the hydrogels during gelation. The average viability of the encapsulated astrocytes was >90% after culture for 14 days (Supplementary Fig. 2a, b), indicating high biocompatibility of the hybrid hydrogels. In addition, decreasing matrix stiffness resulted in a reduced proliferation rate of astrocytes (Supplementary Fig. 2c, d). Further, the proliferation rate of astrocytes decreases during culture, consistent with previous studies[32].

Several studies have shown that after brain injuries, naive astrocytes transform into reactive astrocytes and contribute to glial scar formation[1,33–36]. It has been reported that matrix stiffness acts is an important factor in astrocytic activation; however, most previous studies on matrix stiffness regulating astrocytic activation were unidirectional and performed in 2D culture[14–16,18–21]. To explore the influences of matrix stiffness on astrocyte activation in 3D, we encapsulated astrocytes into hybrid hydrogels of different stiffnesses (i.e., stiff, moderate and soft), which were cultured for 7 days. From F-actin staining (Supplementary Fig. 3), we found that astrocytes cultured in the stiff matrix showed a round morphology with a smaller spreading area, while astrocytes in the softer matrix showed characteristic hypertrophy of cell bodies with a much larger spreading area and a prominent stretched morphology (Fig. 1b). In addition, the cell shape index of astrocytes dropped significantly with decreasing matrix stiffness (Fig. 1c). We further observed that astrocytes cultured in soft hydrogels showed significantly upregulated expression of GFAP and IL-1β compared to those cultured in stiff hydrogels for 7 and even 14 days. (Fig. 1d, e, and Supplementary Figs. 4, 5). The higher expression levels of GFAP in the soft matrix were further confirmed by Western blot analysis (Fig. 1f). Collectively, these results suggest that the phenotype and activation of astrocytes in 3D can be regulated by matrix stiffness.

To confirm this result, we seeded astrocytes on stiff, moderate and soft matrices. We found that astrocytes seeded on the soft matrix showed a reactive phenotype with upregulated GFAP, while astrocytes seeded on the stiff matrix restored the naive phenotype with rounded morphology and low expression of GFAP (Supplementary Fig. 6). The results proved that matrix stiffness does have a strong influence on the activity of astrocytes under both 2D and 3D conditions. In particular, the soft matrix activates astrocytes from a naive phenotype to a reactive phenotype.

Dynamic changes in matrix stiffness switch the astrocyte phenotype

To exploit the effects of dynamically changing matrix stiffness on astrocyte phenotypic switching, we first cultured astrocytes in stiff and soft matrices for 7 days individually. Then, we softened the stiff matrix in situ and stiffened the soft matrix. The astrocyte phenotype was evaluated after another 7 days of culture after dynamic softening or stiffening of the matrix. We observed that astrocytes switch from a naive to a reactive phenotype after softening the stiff matrix by decrosslinking alginate with sodium citrate (Fig. 2) and from a reactive to a naive phenotype after stiffening the soft matrix by crosslinking alginate with calcium chloride (Fig. 3). Specifically, astrocytes cultured in the stiff matrix maintained a naive phenotype with a rounded morphology and low expression of astrocyte markers (GFAP and IL-1β) in the first 7 days of culture. After softening the stiff matrix, astrocytes switch to a typical reactive phenotype with hypertrophy of cell bodies (Supplementary Fig. 7a), an increased spreading area (Fig. 2b) and significantly upregulated the expression of GFAP and IL-1β (Fig. 2d, e). In addition, the higher expression levels of GFAP in the soft matrix were further confirmed by Western blot analysis (Fig. 2f), where the expression of GFAP in the softened matrix was ~1.5 times higher than that in the stiff matrix. In addition, we found that astrocytes reverted to a native phenotype after stiffening the soft matrix (Fig. 3 and Supplementary Fig. 7b). Taken together, our results indicate that dynamic changes in matrix stiffness can switch the astrocyte phenotype in 3D; specifically, matrix softening induces astrocyte activation, while matrix stiffening reverts the activation of astrocytes.

To explore the effect of chemical components, such as calcium chloride and sodium citrate, on astrocyte behavior, P1 astrocytes were seeded at a density of 1×10^4 cells/cm^2 on plastic culture plates and treated individually with 10 mM calcium chloride and 10 mM sodium citrate for 30 min. Since astrocytes spread over the plate in 5 days, we compared the GFAP expression of cells in the experimental

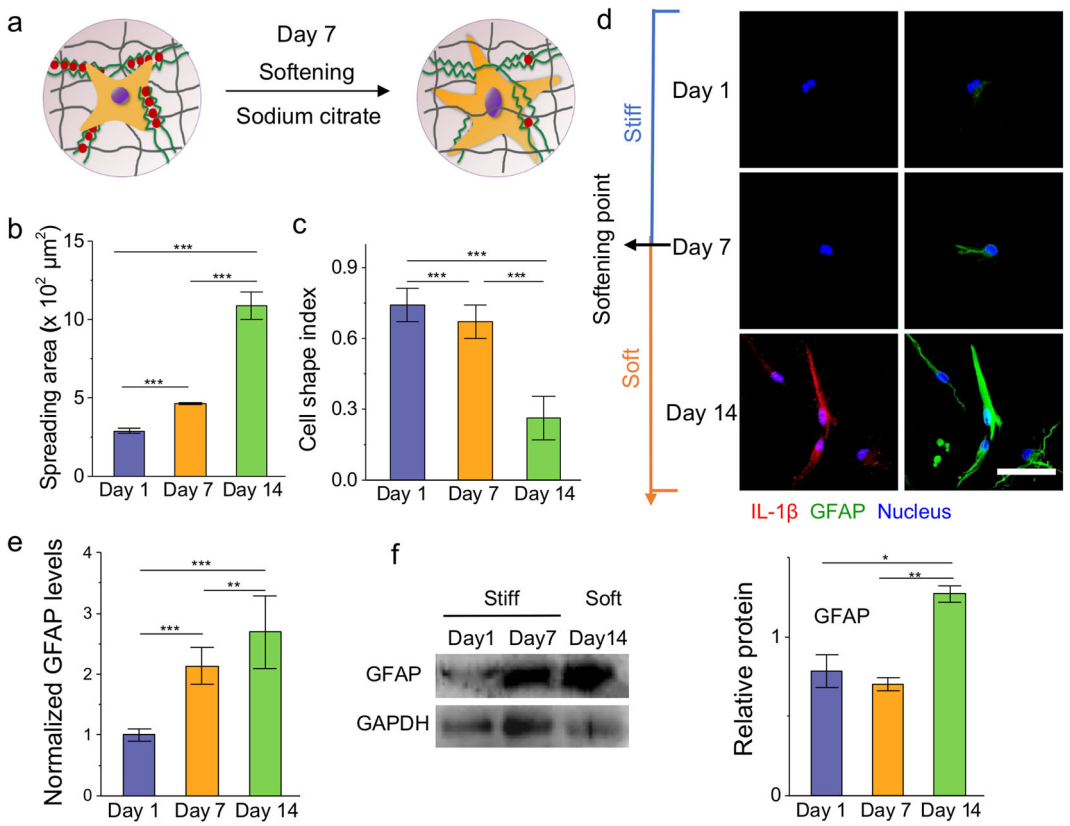

Fig. 2 Matrix softening induced astrocyte activation. a Schematic depiction of matrix softening. **b** The cell spreading area significantly increased when the matrix was softened after 7 days of culture. **c** Matrix softening influenced the shape of astrocytes. **d**, **e** Immunofluorescence analysis indicated that the activation of astrocytes increased when the matrix was softened after 7 days (red, IL-1β; green, GFAP; blue, nucleus). Scale bar, 50 μm. **f** Relative protein levels of GFAP determined by Western blotting in astrocytes after 7 days and 14 days of culture.

groups after culture for 1, 3, and 5 days with the no treatment control group (Supplementary Fig. 8). We found that neither calcium chloride nor sodium citrate had a significant influence on the phenotype of astrocytes, as reflected by GFAP levels (Supplementary Fig. 8b, c).

Since we added 10% (wt/vol) alginate and an equal volume of 10 mM calcium chloride into the soft hydrogel to stiffen the soft hydrogel, it was important to clarify whether the excess alginate would cover the RGD domain in the collagen, which may prevent adhesion and extension of the cells. We seeded P1 astrocytes in hybrid hydrogels containing 5% (wt/vol) and 10% (wt/vol) alginate (final concentrations of 5%, 10% (wt/vol) alginate, 1 mg/mL collagen, and 0 mM Ca^{2+}). We first measured the stiffness of both hydrogels and found no significant difference between the two hydrogels (Supplementary Fig. 9b). According to the analysis of GFAP expression, we found that excess uncrosslinked alginate did not prevent the reactivity of astrocytes, and there was also no significant difference between the two groups (Supplementary Fig. 9a, c). Together, our data proved that the added chemicals and excess uncrosslinked alginate did not affect the phenotype of astrocytes. It is only the stiffness of the substrate that regulates astrocyte phenotype in 3D.

Although matrix stiffness clearly regulates astrocyte phenotypic transformation[18], the underlying mechanoregulatory pathways are still poorly understood. In the 3D hybrid hydrogel system, we noticed that the enhanced activation of astrocytes in the soft matrix was always accompanied by an extended spreading area (Supplementary Figs. 3, 7). According to previous studies, matrix stiffness affects cell fate and behavior by changing cytoskeletal tension[37–40] and rapidly remodeling the cytoskeleton[41]. To test this possibility, we first cultured astrocytes on stiff matrix for 3 days, treated astrocytes with a series of concentrations of blebbistain to inhibit cytoskeletal tension to different degrees and cultured the astrocytes until the 14th day. Our data suggest that astrocytes treated with blebbistain exhibit an extended spreading area and filopodium-rich morphology along with significant upregulation of GFAP (Supplementary Fig. 10). Moreover, the influence of blebbistain on astrocyte activation is dependent on both dose and time. Thus, the inhibition of cytoskeletal tension induces the activation of astrocytes,

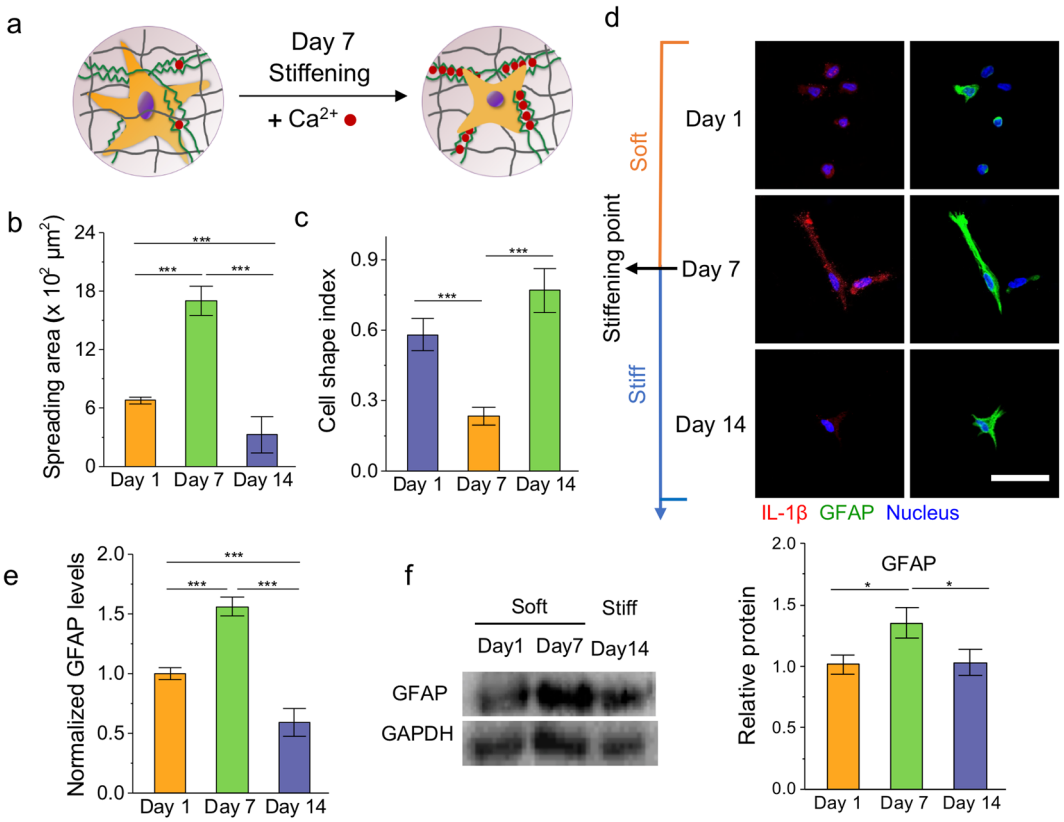

Fig. 3 Matrix stiffening reverted the activation of astrocytes. a Schematic depiction of matrix stiffening. **b** The cell spreading area significantly decreased when the matrix was stiffened after 7 days of culture. **c** Matrix stiffening influenced the shape of astrocytes. **d**, **e** Immunofluorescence analysis indicated that the activation of astrocytes decreased when the matrix was stiffened after 7 days (red, IL-1β; green, GFAP; blue, nucleus). Scale bar, 50 μm. **f** Relative protein levels of GFAP determined by Western blotting in astrocytes after 7 days and 14 days of culture.

suggesting that matrix stiffness might affect astrocyte activation by regulating cytoskeletal tension.

YAP inhibition enhances the responses of astrocytes to matrix stiffness

YAP[42,43], a key regulator in multiple organ development[44], is highly expressed in astrocytes in vivo. To test whether YAP activity is regulated by matrix stiffness, we characterized the expression of YAP in astrocytes cultured in stiff and soft matrices. We found that astrocytes cultured in the stiff matrix displayed higher levels of YAP expression than those cultured in the soft matrix after 7 days of culture. We also noticed that the nuclear localization of YAP was increased in astrocytes cultured in the stiff matrix (Fig. 4a–d). Then, we analyzed the expression of YAP and GFAP in astrocytes cultured in matrix with dynamic stiffness changes. We found that astrocytes in the stiff matrix maintained a naive phenotype with low expression of GFAP and rather high activity of YAP, while after matrix softening, naive astrocytes switched to reactive astrocytes with upregulated GFAP and decreased YAP expression (Fig. 4a). In addition, the corresponding phenotypic transformation of astrocytes was also observed when stiffening the soft matrix (Fig. 4b). The results indicate that the expression of YAP is sensitively regulated by matrix stiffness and its dynamic changes. They also indicate that YAP could be involved in the responses of astrocyte phenotype switching to dynamically changing matrix stiffness.

To gain insight into the role of YAP in the responses of astrocytes to matrix stiffness, we transfected astrocytes cultured for 3 days with siRNAs targeting YAP (SiYAP) to inhibit the expression of YAP. Four days later, we found that astrocytes transfected with SiYAP showed enhanced activation with upregulation of GFAP in the stiff matrix compared to the control group (Fig. 4e, f). These results indicate that YAP might be a key factor in the response of astrocytes to matrix stiffness.

The mathematical modeling results suggest that GFAP expression is more sensitive to biomolecules associated with the cytoskeleton and nucleus

To investigate the underlying mechanism by which matrix stiffness affects GFAP expression, we also

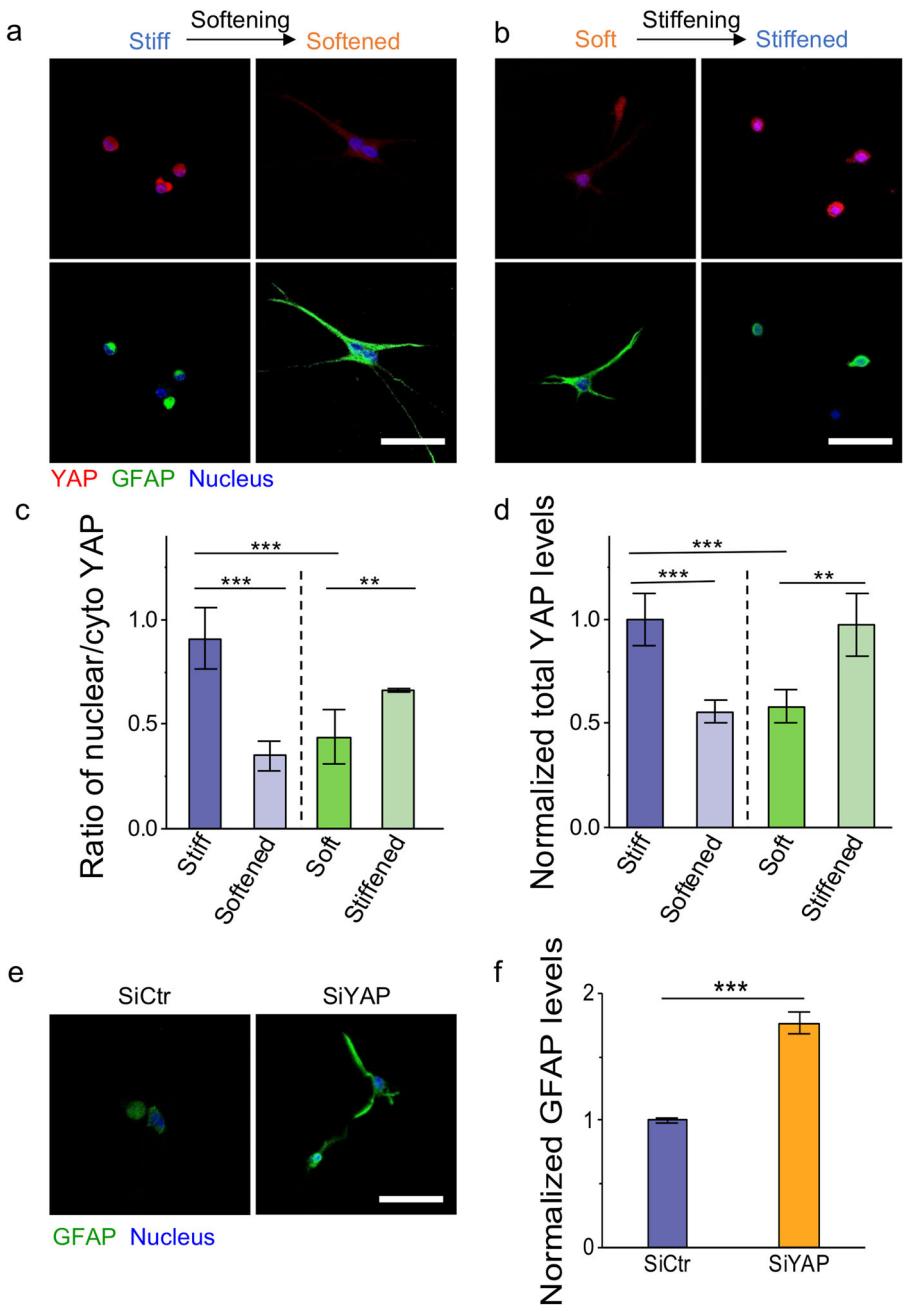

Fig. 4 YAP inhibition enhanced the responses of astrocytes to matrix stiffness. a, **b** Immunofluorescence analysis suggested that increasing matrix stiffness reduced the expression of the YAP protein and upregulated the expression of the GFAP protein (red, YAP; green, GFAP; blue, nucleus). Scale bar, 50 μm. **c** Quantification of the ratio of nuclear YAP to cytoplasmic YAP in astrocytes. **d** Quantification of the normalized total YAP levels. **e** Immunofluorescence analysis indicated that astrocyte activation increased when astrocytes in a stiff matrix were transfected with siRNAs targeting YAP (blue, nucleus; green, GFAP). Scale bar, 50 μm. **f** Quantification of GFAP levels when astrocytes in a stiff matrix were transfected with siRNAs targeting YAP.

developed a mathematical model consisting of a series of ordinary differential equations (ODEs) that describe the time-dependent dynamics of biomolecular interactions[45,46]. The modeling results showed that a stiff matrix inhibits the expression of GFAP through the activation of YAP. We further compared the predicted normalized GFAP levels from our mathematical model (Fig. 5c) with the experimental results (Fig. 1d, e). We found that the modeling and experimental results were consistent.

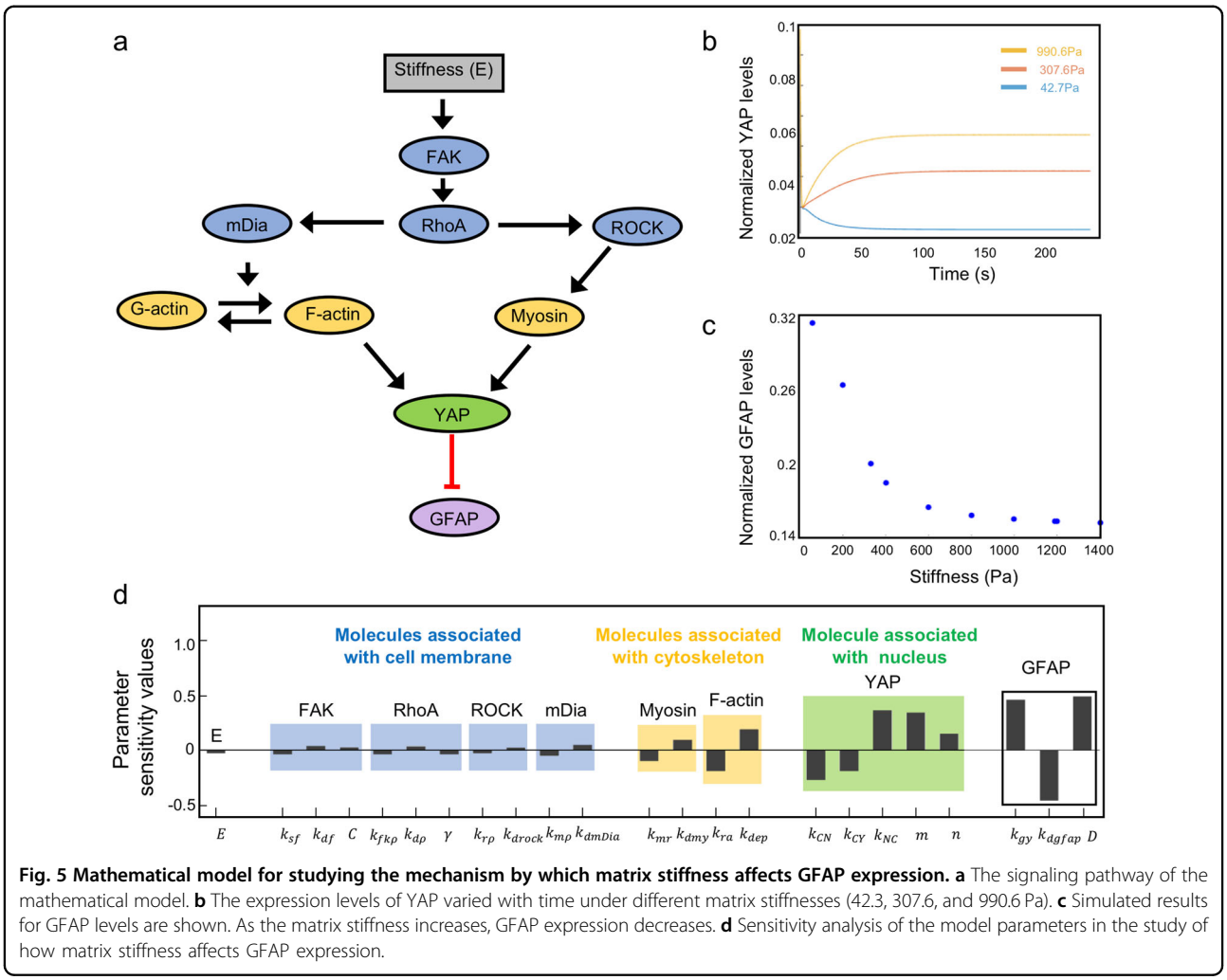

Fig. 5 Mathematical model for studying the mechanism by which matrix stiffness affects GFAP expression. a The signaling pathway of the mathematical model. **b** The expression levels of YAP varied with time under different matrix stiffnesses (42.3, 307.6, and 990.6 Pa). **c** Simulated results for GFAP levels are shown. As the matrix stiffness increases, GFAP expression decreases. **d** Sensitivity analysis of the model parameters in the study of how matrix stiffness affects GFAP expression.

To evaluate the roles of intracellular signaling dynamics in matrix stiffness-mediated GFAP expression in astrocytes, we performed parameter sensitivity analysis using the developed mathematical model (Fig. 5d). We divided the parameters into the following three categories according to the key biomolecules involved in mediating GFAP expression: (1) molecules associated with the cell membrane; (2) molecules associated with the cytoskeleton; and (3) molecules associated with the nucleus. The sensitivity analysis of parameters showed that parameters related to the cytoskeleton and nucleus have a greater impact on GFAP expression. Based on this, we speculate that matrix stiffness may induce changes in cytoskeletal tension, which may further affect the activity of YAP and thus GFAP expression. This is consistent with the results reported in the literature[20,37–42,47].

Discussion

Reactive astrogliosis, which ultimately forms glial scars, was not thought to be reversible until an in vivo study revealed the microenvironment-dependent plasticity of astrocyte phenotypes, where reactive astrocytes could revert in retrograde to naive astrocytes in an appropriate microenvironment[14]. We first proved the plasticity of astrocyte phenotypes in a 3D in vitro model from a mechanobiological perspective. Our findings show that matrix stiffness is a vital microenvironmental cue that impacts astrocyte phenotypic transformation. We found that astrocytes developed an activated phenotype in soft hydrogels but maintained an inactive phenotype in stiff hydrogels (Fig. 1d–g). Interestingly, stiffening of soft hydrogels reverted the activation of astrocytes, whereas softening of the stiff matrix induced astrocyte activation (Figs. 2, 3). Thus, we linked the phenotypic transformation of astrocytes to dynamic changes in matrix stiffness for the first time. Moreover, according to an in vivo study, glial scars in the rat cortex are significantly softer than healthy CNS tissues, as measured by atomic force microscopy[6]. Our results therefore mimic this phenomenon and suggest that the softer components of the ECM (such as highly hydrated CSPGs) increase in abundance during scar

formation, which may induce astrocyte activation. Furthermore, this reactive astrogliosis could be reverted when the matrix environment is restored to the preinjury structure.

Collagen is produced when the CNS is injured[48,49]. We noted that during CNS scar formation, the stiffness of the CNS also changes. Both the changed collagen content and matrix stiffness could contribute to astrocyte activation and scar formation. While collagen has been widely used as an ECM mimic for culturing diverse types of cells (including astrocytes), the effects of matrix stiffness changes on astrocyte behavior in pathological conditions remain unclear. Therefore, we used collagen as a representative matrix in pathological conditions for culturing astrocytes. Because it is inherently bioactive and easy to obtain, collagen has been applied as a brain engineering scaffold for diverse clinical indications. For instance, bioengineered brain-like cortical tissue based on collagen type I gel and silk scaffolds promoted neuron anchoring and the formation of neural networks[50]. Collagen type I was used in coculturing endothelial cells, pericytes, and astrocytes to model the blood–brain barrier in 3D[51]. Moreover, neural progenitors cultured in collagen type I gels showed significantly higher survival and neuronal differentiation than those cultured on 2D gels[52]. Additionally, astrocytes seeded in the collagen type I system remained in a low reactive state, resembling their status in the healthy CNS[28,29]. We acknowledge that simply using collagen is not sufficiently representative of the complex CNS matrix in pathological conditions. Hyaluronic acid and laminin could be incorporated into collagen to better establish pathological relevance systems[53–56]. Further work is needed to investigate this.

In addition, to decouple the effects of matrix stiffness from collagen content, we used Ca^{2+}-crosslinked alginate (an inherently bioinert material) to dynamically tune the mechanical properties of the hydrogel without significantly changing the collagen content or structure. It is important to develop new methods and material systems to independently tune the mechanical properties of hydrogels, avoiding the use of nonnative ECM components such as alginate.

Injury to the CNS activates naive astrocytes to reactive astrocytes. Recent evidence has indicated that reactive astrocytes can be further differentiated into A1 reactive astrocytes and A2 reactive astrocytes according to their functions[57–62]. The toxic A1 phenotype, which can be marked by complement component 3 (C3), induces neuronal death and shows a broader relevance to neurodegenerative diseases[57–60,62,63]. In addition, neuroprotective A2 astrocytes, marked by S100A10, contribute to protecting neurons and repairing damage[61,63]. In this study, we mainly focused on the process from of activation from naive astrocytes to reactive astrocytes. We actually did not aim to distinguish reactive astrocytes from the A1 phenotype to the A2 phenotype. To characterize the ratio of type A1 or type A2 astrocytes to total cells, astrocytes enveloped in both stiff and soft hybrid hydrogels were subjected to colocalization of C3 and S100A10 after culture for 1 and 7 days. We found that A2 reactive astrocytes were very rare in each group (almost none). After 7 days, the number of cells of the A1 phenotype significantly increased in the soft hydrogel compared to the stiff hydrogel (Supplementary Fig. 11), which matched the results shown in Fig. 1d and Supplementary Fig. 4. In particular, rare astrocytes seeded in stiff hydrogels were marked by C3 or S100A10 on day 1, which means that the astrocytes maintained a naive phenotype, consistent with the results in Fig. 1d and Supplementary Fig. 4. Our results also proved that astrocytes were naive at the beginning of the experiments.

In addition to the characteristic marker GFAP, we also chose the IL-1β protein to reflect the inflammatory response of astrocytes. IL-1β is widely regarded as the top level of the cascade of neuroinflammatory mediators[13,64] and is associated with astrocyte activation[65–67]. In this work, we found that astrocytes cultured in soft hydrogels showed significantly upregulated expression of IL-1β and GFAP (Fig. 1d). A recent study reported that A1 reactive astrocytes could increase their expression of proinflammatory cytokines, such as IL-1β[68]. We also detected that most of the reactive astrocytes were A1 type (Supplementary Fig. 11), which is consistent with our results (Fig. 1d and Supplementary Figs. 4, 5).

Matrix stiffness affects cell fate and behavior by changing cytoskeletal tension and rapidly remodeling the cytoskeleton. In our study, we observed that a stiff matrix prevents the spreading of astrocytes along with low expression of GFAP. The inhibition of cytoskeletal tension induced the activation of astrocytes cultured on stiff matrix, exhibiting an extended spreading area, filopodium-rich morphology, and significant upregulation of GFAP (Supplementary Fig. 10). This implies that cytoskeletal tension might be involved in the regulation of the astrocyte phenotype by matrix stiffness.

YAP, a key regulator in multiple organ development, has been reported to be associated with negative control of reactive astrogliosis. Our results indicate that the activity of YAP is regulated by matrix stiffness and its dynamic changes (Fig. 4a–d). Further exploration proved that the decrease in YAP expression enhances reactive astrogliosis with upregulation of GFAP (Fig. 4e, f), which indicates that YAP might be a critical factor for the astrocyte response to dynamically changing matrix stiffness. Combining the sensitivity analysis with the mathematical model, we speculate that matrix stiffness may induce changes in cytoskeletal tension, which may further affect the activity of YAP and thus the astrocytic phenotype (through GFAP expression). Thus, these findings suggest the potential mechanism by which matrix stiffness regulates astrocyte phenotypic transformation.

Matrix stiffness has been proven to be a major mechanical cue in modulating cell behaviors, for example, governing stem cell fate[69]. Cells cense dynamic mechanical changes via deformation and reorganization of the microtubule cytoskeleton, and the degree of matrix stiffening determines cell fate[69]. Our results support this point, and we found that astrocyte fate can be controlled by matrix stiffness in a 3D microenvironment. In addition to matrix stiffness, dynamic architectural features of hydrogel networks could also be involved in regulating the astrocytic phenotype[18]. Here, we decouple the mechanical and structural changes of hydrogels and clarify the effect of the mechanical response (dynamically changed matrix stiffness) of hydrogels on cell phenotypic transformation. Our hydrogel system imitates the modulus (~40–1000 Pa) of both healthy and injured brain tissues in vivo and provides a physiologically relevant 3D microenvironment for astrocytes, which allows us to assess the impact of dynamically changing stiffness on astrocytic phenotypic transformation. Moreover, the dynamic hydrogel system would contribute to further explorations of the engineering of dynamic cellular microenvironments.

Conclusions

In this study, we established an in vitro model to assess the responses of astrocytes to matrix stiffness changes that may be related to pathophysiology. We found that astrocytes exhibit different phenotypes when cultured in hydrogels of different stiffnesses. More importantly, the adopted phenotypes can be switched in situ when matrix stiffness is changed in the presence of cells, i.e., the cells can adapt to the in situ changes in matrix stiffness by switching their phenotypes. Specifically, we showed that matrix stiffening can revert astrogliosis, whereas matrix softening induces astrocyte activation in 3D. We also revealed that YAP is involved in matrix stiffness-regulated astrocyte activation, where the inhibition of YAP induces the upregulation of GFAP and contributes to astrogliosis. We further developed a mathematical model to study the underlying mechanism by which matrix stiffness affects GFAP expression, and the modeling results were consistent with the experimental results. The findings from this study may enhance the understanding of the role of mechanical cues in reactive astrogliosis and inspire the development of a potential therapeutic approach for controlling glial scar formation following injury from the mechanobiological perspective.

Materials and Methods

Construction of the switchable hydrogel system

To synthesize hybrid hydrogels with tunable stiffness, 20% (wt/vol) alginate and 4 mg/mL collagen type I were first mixed before adding $CaSO_4$ suspension (0, 8, and 20 mM, respectively) and cell culture medium to reach a final concentration of 5% (wt/vol) alginate, 1 mg/mL collagen, and 0/2/5 mM Ca^{2+}. The mixture was then incubated for 45 min at 37 °C to allow crosslink formation. Following the literature[27], hydrogel softening was achieved by chelating Ca^{2+} with 100 mM sodium citrate for 30 min at 37 °C to dissolve alginate, followed by washing with cell culture medium. To stiffen the hydrogels, 10% (wt/vol) alginate was added on the surface of soft hydrogels. After 45 min of infiltration at 37 °C, the excess alginate was removed, and an equal volume of 10 mM calcium chloride was added to crosslink alginate infiltrated into the collagen.

Mechanical characterization

To test the rheology of the hybrid hydrogels, samples were prepared as disks with a diameter of 8 mm and a thickness of 2 mm. Before rheological testing, the hybrid hydrogels were soaked in PBS for 24 h. At the beginning of the test, the plate slowly descended until reaching the normal force of ~20 mN. Frequency tests were applied with a strain of 0.5% and a frequency ranging from 0.1 to 10 rad/s. The storage modulus and loss modulus were calculated from the average of the modulus between frequencies of 0.25 and 2.5 rad/s, where the modulus maintained a balanced value.

A simple magnetic tweezer device was used to determine the modulus of the material. Briefly, an electromagnet with a sharp-tipped nickel alloy core generated a strong magnetic field gradient, thus creating an attractive force on the bead that points toward the tip. The magnetic force applied on the bead was calibrated according to the speed of the beads in a viscous liquid as a function of the tip-to-bead distance. Bead positions were recorded by a CCD camera and tracked using a grayscale binarized center-of-mass algorithm in MATLAB. The strain (ε) of the materials was defined as the ratio of the displacement of the beads (x) to the diameter of the beads ($2R$), and the stress (σ) was defined as the ratio of the applied magnetic force (F) to the maximum cross-sectional area of the beads:

$$\varepsilon = \frac{x}{2R} \tag{1}$$

$$\sigma = \frac{F}{\pi R^2} \tag{2}$$

Then, the modulus of the material (E) was calculated as:

$$E = \frac{\sigma}{\varepsilon} \tag{3}$$

Structural characterization

After being fixed with 2.5% glutaraldehyde for 2 h, all samples were dehydrated by exposure to a graded series of

ethanol-*t*-butanol mixtures (ethanol/*t*-butanol = 70/30, 50/50, 30/70, 20/80, and 10/90 for 10 min each) before being treated with pure *t*-butanol. After being dried by a freeze dryer, the samples were coated with gold. Imaging was performed by employing a MAIA3 LMH field emission SEM at 15 kV accelerating voltage.

Swelling performance

After freeze-drying, the dry weight (W_d) of the samples was determined by using an electronic precision balance. After that, the samples were placed in PBS to swell for 24 h at room temperature. The surface moisture of the samples was removed by filter papers before weighing the wet weight (W_w) of the samples. The swelling ratio of the samples was calculated as $(W_w - W_d)/\mathrm{Wd} \times 100\%$.

Primary astrocyte isolation and 3D culture

All Sprague-Dawley (SD) rats used in the present study were obtained from the Laboratory Animal Center of Xi'an Jiaotong University Health Science Center, China. All procedures and ethics guidelines were approved by the Committee for Experimental Animal Use and Care of Xi'an Jiaotong University Health Science Center, China. Astrocytes were collected from the cortex of neonatal rats (1 day old). Briefly, the cortical tissues of neonatal rats were dissociated with trypsin, and cells were plated in a 75 cm^2 flask (Thermo Fisher Scientific, USA) in Dulbecco's modified Eagle's medium with F-12 nutrient mixture (DMEM/F-12; HyClone, USA) containing 10% fetal bovine serum (FBS; Gibco, USA), 1% penicillin-streptomycin (Pen-Strep; Gibco, USA) at 37 °C and 5% CO_2. After 24 h, the culture medium was changed twice per week. Cultures were shaken at 300 rpm/min for 12–18 h to remove other types of neuronal cells after 10 days. All experiments were performed using astrocytes from the first passage (P1). P1 cells were seeded at a density of 1×10^6 cells/mL in combined hydrogels and cultured in DMEM/F-12 medium containing 10% FBS and 1% Pen-Strep for 7 or 14 days.

Characterization of cell viability

For cell viability experiments, samples were incubated in 1 mL of PBS containing 0.5 μL of Calcein-AM (Life Technologies, USA) and 2 μL of EthD-1 (Life Technologies, USA) for 15 min at 37 °C and 5% CO_2, followed by three washes with PBS. Imaging was performed with an OLYMPUS IX81 inverted phase contrast fluorescence microscope. Live and dead cells were counted by using a cell counter plug-in for ImageJ.

Immunofluorescence staining

Samples were fixed in 4% paraformaldehyde for 20 min and washed in PBS three times for 5 min before penetrating samples with 0.5% Triton X-100 (Sigma, USA) for 15 min and washed in PBS three times for 5 min. Samples were then incubated in PBS containing 10% normal goat serum (Thermo Fisher Scientific, USA) and 5% bovine serum albumin (BSA; MP Biomedicals, USA) for 1 h. Samples were incubated in primary antibodies prepared in proper dilutions in PBS containing 1% BSA overnight at 4 °C. After washing with PBS, the samples were incubated with appropriate Alexa 488 or Alexa 594 secondary antibodies (1:400, Thermo Fisher Scientific, USA). To visualize F-actin, samples were stained with Alexa 488-labeled phalloidin for 1 h. The following primary antibodies were used for immunofluorescence: rabbit anti-IL-1β (inflammatory marker, 1:100; Abcam, ab9722, USA), mouse anti-GFAP (1:400; Cell Signaling Technology, 3670, USA), rabbit anti-Ki67 (proliferation marker, 1:400; Cell Signaling Technology, 9129, USA), rabbit anti-S100A10 (1:500; Bioss, bs-8503R, China), mouse anti-C3 (1:200; Santa Cruz, sc-8399, USA), and rabbit anti-YAP (1:100; Cell Signaling Technology, 14074, USA). After labeling nuclei with DAPI (1 μg/mL; Sigma, D9542, USA) for 10 min, fluorescence images were taken with an Olympus FV3000 laser scanning confocal microscope.

Cell shape index

Based on the F-actin immunofluorescence staining of samples, the cell shape index was analyzed with Fuji software (ImageJ); the higher the cell shape index was, the closer to a circle the cell was.

$C = 4\_\mathrm{pi}\_A/P\text{^}2 - 12.57\_A/P\text{^}2$, where C is the circularity, A is the area, and P is the perimeter.

Characterization of normalized protein levels

Confocal images were taken with distinct z-stacks. For all the samples, the distance between two z-stacks was set to the same value. For the quantitative analysis of GFAP, YAP and nuclear localization of YAP, the fluorescence intensity of all images was set to the same parameter. The normalized protein levels of the samples were analyzed by Fuji software with the Image plugin.

Cell transfection and inhibition

Astrocytes were cultured in hydrogels for 3 days, and then YAP knockdown was performed in astrocytes by using a small interfering RNA (siRNA). Control cells were transfected with control siRNA (5′-UUCUCCGAACGUGUC ACGUTT). siRNA transfections were performed with Lipofectamine™ 2000 (Life Technologies, USA) in Opti-MEM I reduced serum medium (Invitrogen, USA) according to the manufacturer's instructions. The target sequence of the siRNA was 5′-GGUCAGAGAUACUUCUUAATT for rat YAP.

Western blotting

For Western blot analysis, protein extracts were obtained from samples cultured after 1, 7, or 14 days. First, the samples were treated with 100 mM sodium

citrate for 30 min to dissolve alginate, followed by washing with PBS. Then, 5 mg/mL type IV collagenase was added to dissolve collagen. The total protein extracts were separated by SDS-polyacrylamide gel electrophoresis and electrotransferred to polyvinylidene difluoride membranes (Millipore, USA). The membranes were blocked with TBST containing 5% BSA and incubated with primary antibodies overnight at 4 °C. The following antibodies were used: rabbit anti-GAPDH (1:1000; Cell Signaling Technology, 2118, USA), GFAP (1:1000; Abcam, USA), and YAP (1:1000; Cell Signaling Technology, 14074, USA). Then, the membranes were washed with TBST five times and incubated with the corresponding secondary antibodies (1:5000; Cell Signaling Technology, USA) for 2 h at room temperature. After being washed with TBST five times, protein signals were detected by using a chemiluminescence system (ChemiScope 3300 mini, China). Densitometry analysis was performed with ImageJ (National Institutes of Health, USA). The analyses were performed in three independent experiments with three replicates per condition.

Statistical analysis

Statistical analysis was conducted by using the OriginPro software package (Origin Pro 2016; Origin Lab, Northampton, USA). Statistics are presented as the mean ± standard deviation for all quantitative data. One-way analysis of variance (ANOVA) was used for two-group comparisons along with a *t*-test ($^{*}p < 0.05$, $^{**}p < 0.01$, and $^{***}p < 0.001$).

Mathematical model

For the sake of simplicity, we assumed that the total amount of each protein can be normalized to 1 in our model. The proteins involved in the signaling pathway in our model contain only two states (i.e., active and inactive states).

The mechanical properties of the ECM are transmitted to intracellular signals via adhesion molecules such as focal adhesion kinase (FAK). Adhesion molecule activation induces the binding of RhoA to GTP. RhoA-GTP drives the formation of actomyosin by mDia and ROCK activation. mDia is a formin that polymerizes F-actin. ROCK can activate myosin. Finally, the resultant F-actin and myosin activity leads to nuclear translocation of YAP[40]. Recently, a study reported that the activation of YAP may inhibit the expression of GFAP[42]. According to the work of Kosako et al. and Goto et al., GFAP was found to be phosphorylated by Rho kinase, resulting in an inhibition of their formation in vitro[70,71]. Guasch et al. showed that astrocytes transfected with active RhoA lack GFAP and vimentin expression[72]. These studies together support the signaling pathway we adopted (Fig. 5a).

To describe this pathway, a set of ODEs were derived. According to the work of Sun et al.[40], the time dependence of active phosphorylated FAK is given by

$$\frac{d\mathrm{FAK}_p(t)}{dt} = k_{\mathrm{sf}}\frac{E^2}{E^2+C^2}\left(\mathrm{FAK}_0 - \mathrm{FAK}_p(t)\right) - k_{\mathrm{df}}\mathrm{FAK}_p(t) \tag{1}$$

Here, k_{sf} is the maximum activation rate due to the ECM, and the dephosphorylation rate of FAK is k_{df}. C is the value of E when the activation rate of FAK is $k_{\mathrm{sf}}/2$, which is one-half of the maximum activation rate[73].

Phosphorylated FAK activates RhoA, and the time dependence of the concentration of RhoA is given by

$$\frac{d\mathrm{RhoA}_{\mathrm{GTP}}(t)}{dt} = k_{\mathrm{fk}\rho}\left(\gamma\left(\mathrm{FAK}_p(t)\right)^2+1\right)\left(\mathrm{RhoA}_0 - \mathrm{RhoA}_{\mathrm{GTP}}(t)\right) - k_{\mathrm{d}\rho}\mathrm{RhoA}_{\mathrm{GTP}}(t) \tag{2}$$

Here, $k_{\mathrm{fk}\rho}$ is the baseline activation rate of RhoA due to molecules other than phosphorylated FAK; $k_{\mathrm{d}\rho}$ is the RhoA-GTP deactivation rate, which is relevant to the hydrolysis rate of RhoA-bound GTP to GDP; and γ is the RhoA activation enhancement due to active FAK[73].

Downstream of RhoA, ROCK, and mDia are activated. Their time-dependent concentration is given by Eqs. (3–4), respectively.

$$\frac{dROCK_A(t)}{dt} = k_{r\rho}RhoA_{GTP}(t)(ROCK_0 - ROCK_A(t)) - k_{drock}ROCK_A(t) \tag{3}$$

$$\frac{d\mathrm{mDia}_A(t)}{dt} = k_{\mathrm{m}\rho}\mathrm{RhoA}_{\mathrm{GTP}}(t)(\mathrm{mDia}_0 - \mathrm{mDia}_A(t)) - k_{\mathrm{dmDia}}\mathrm{mDia}_A(t) \tag{4}$$

Here, $k_{r\rho}$ is the activation rate of ROCK due to RhoA-GTP, k_{drock} is the deactivation rate of ROCK, $k_{\mathrm{m}\rho}$ is the activation rate of mDia due to RhoA-GTP, and k_{dmDia} is the deactivation rate of mDia[73].

Myosin is then upregulated by ROCK and evolves according to:

$$\frac{d\mathrm{Myo}_A(t)}{dt} = k_{\mathrm{mr}}\mathrm{ROCK}_A(t)\left(\mathrm{Myo}_0 - \mathrm{Myo}_A(t)\right) - k_{\mathrm{dmy}}\mathrm{Myo}_A(t) \tag{5}$$

Here, k_{mr} is the activation rate of myosin due to pathways other than ROCK, k_{dmy} is the deactivation rate of myosin, and ε is the myosin activation enhancement due to active ROCK[73].

For simplicity, the ratio between G-actin and cortical F-actin is assumed to be constant. Cytoplasmic F-actin is

regulated by mDia as follows:

$$\frac{dF\mathrm{cyto}(t)}{dt} = k_{\mathrm{ra}}\mathrm{mDia}_A(t)\mathrm{Gactin}(t) - k_{\mathrm{dep}}F\mathrm{cyto}(t) \tag{6}$$

Here, k_{ra} is the polymerization rate of cytoplasmic F-actin from G-actin, and k_{dep} is the depolymerization rate of cytoplasmic F-actin[73].

YAP is regulated by cytoplasmic F-actin and myosin activity. It translocates to the nucleus to bind with transcription factors and activates them. The nuclear YAP concentration is given by

$$\frac{dY\mathrm{AP}_N(t)}{dt} = (k_{\mathrm{CN}} + k_{\mathrm{CY}}[F\mathrm{cyto}(t)]^m[\mathrm{Myo}_A(t)]^n)(Y\mathrm{AP}_0 - Y\mathrm{AP}_N(t)) - k_{\mathrm{NC}}Y\mathrm{AP}_N(t) \tag{7}$$

Here, k_{CN} is the rate of YAP translocation from the cytoplasm to the nucleus with no active cytoplasmic F-actin and myosin; k_{NC} is the rate of YAP translocation from the nucleus to the cytoplasm; and k_{CY} is the YAP nuclear translocation rate due to stress fibers or tensional cytoplasmic F-actin. The value m characterizes the weight of how YAP activity is dependent on cytoplasmic F-actin. The value n characterizes the extent to which YAP activity is dependent on myosin. The values $n = 1$ and $m = 1$ are the default settings that indicate that myosin and cytoplasmic F-actin have a similar ability to regulate YAP activity[73].

Recently, it was reported that the activation of YAP may inhibit the expression of GFAP[42]; thus, GFAP expression is given by:

$$\frac{d\mathrm{GFAP}(t)}{dt} = k_{\mathrm{gy}}\frac{D^2}{D^2 + Y\mathrm{AP}_N(t)^2}(\mathrm{GFAP}_0 - \mathrm{GFAP}(t)) - k_{\mathrm{dgfap}}\mathrm{GFAP}(t) \tag{8}$$

Here, k_{gy} is the inhibition rate due to YAP, and the dephosphorylation rate of GFAP is k_{dgfap}. D is a constant.

The values for the parameters used in the non-dimensionalized model are shown in Table S1[73,74].

The sensitivity value S of the level of GFAP to a parameter p is defined in the equation below, where p is the base parameter value, and C_{GFAP} is the level of GFAP[74,75].

$$S = \frac{\mathrm{dlog}(C_{\mathrm{GFAP}})}{\mathrm{dlog}(p)} \tag{9}$$

The S value is equivalent to the slope of CGFAP versus p on a log-log plot and represents the fold change in the level of GFAP resulting from a fold change in a parameter value. The S value was calculated by plotting CGFAP at 0.1-, 1-, and 10-fold changes of the base parameter on a log-log scale. A line was fitted to the data points with the slope of the line taken to be the S value.

Acknowledgements
This work was financially supported by the National Natural Science Foundation of China (11522219, 11872298, 11761161004, 81960786, and 31900939) and the China Postdoctoral Science Foundation (2019T120895).

Author details
[1]The Key Laboratory of Biomedical Information Engineering of Ministry of Education, Xi'an Jiaotong University, Xi'an 710049, P.R. China. [2]Bioinspired Engineering and Biomechanics Center (BEBC), Xi'an Jiaotong University, Xi'an 710049, P.R. China. [3]Department of Engineering Mechanics, School of Civil Engineering, Wuhan University, Wuhan 430072, P.R. China. [4]Department of Neurosurgery, Tangdu Hospital, The Fourth Military Medical University, Xi'an 710038, P.R. China. [5]Jishou University, Jishou 416000, P.R. China

Conflict of interest
The authors declare no competing interests.

Supplementary information The online version contains supplementary material available at https://doi.org/10.1038/s41427-021-00304-0.

Received: 18 June 2020 Revised: 17 February 2021 Accepted: 3 March 2021.
Published online: 16 April 2021

References

1. Rolls, A., Shechter, R. & Schwartz, M. The bright side of the glial scar in CNS repair. *Nat. Rev. Neurosci.* **10**, 235–241 (2009).
2. Yiu, G. & He, Z. Glial inhibition of CNS axon regeneration. *Nat. Rev. Neurosci.* **7**, 617–627 (2006).
3. Fitch, M. T. & Silver, J. CNS injury, glial scars, and inflammation: inhibitory extracellular matrices and regeneration failure. *Exp. Neurol.* **209**, 294–301 (2008).
4. Anderson, M. A. et al. Astrocyte scar formation aids central nervous system axon regeneration. *Nature* **532**, 195 (2016).
5. Patel, D. C., Tewari, B. P., Chaunsali, L. & Sontheimer, H. Neuron–glia interactions in the pathophysiology of epilepsy. *Nat. Rev. Neurosci.* **20**, 1 (2019).
6. Moeendarbary, E. et al. The soft mechanical signature of glial scars in the central nervous system. *Nat. Commun.* **8**, 14787 (2017).
7. Chedly, J. et al. Physical chitosan microhydrogels as scaffolds for spinal cord injury restoration and axon regeneration. *Biomaterials* **138**, 91 (2017).
8. Jha, M. K., et al. Functional dissection of astrocyte-secreted proteins: Implications in brain health and diseases. Progress in Neurobiology 162 (2017).
9. Roitbak, T. & Syková, E. Diffusion barriers evoked in the rat cortex by reactive astrogliosis. *Glia* **28**, 40–48 (1999).
10. Eng, L. F. & Ghirnikar, R. S. GFAP and astrogliosis. *Brain Pathol.* **4**, 229–237 (2010).
11. Vos, P. E. et al. GFAP and S100B are biomarkers of traumatic brain injury: an observational cohort study. *Neurology* **75**, 1786–1793 (2010).
12. Pekny, M. & Nilsson, M. Astrocyte activation and reactive gliosis. *Glia* **50**, 427–434 (2005).
13. Moshayedi, P. et al. The relationship between glial cell mechanosensitivity and foreign body reactions in the central nervous system. *Biomaterials* **35**, 3919–3925 (2014).

14. Hara, M. et al. Interaction of reactive astrocytes with type I collagen induces astrocytic scar formation through the integrin–N-cadherin pathway after spinal cord injury. *Nat. Med.* **23**, 818 (2017).
15. Wilson, C. L., Hayward, S. L. & Kidambi, S. Astrogliosis in a dish: substrate stiffness induces astrogliosis in primary rat astrocytes. *RSC Adv.* **6**, 34447–34457 (2016).
16. Pogoda, K. et al. Compression stiffening of brain and its effect on mechanosensing by glioma cells. *N. J. Phys.* **16**, 075002 (2014).
17. Tavakol, S. et al. Mechano-transduction signals derived from self-assembling peptide nanofibers containing long motif of laminin influence neurogenesis in in-vitro and in-vivo. *Mol. Neurobiol.* **54**, 1–14 (2016).
18. Freeman, R. et al. Reversible self-assembly of superstructured networks. *Science* **362**, 808–813 (2018).
19. Tavakol, S., Mousavi, S. M. M., Tavakol, B., Hoveizi, E. & Sorkhabadi, S. M. R. Mechano-transduction signals derived from self-assembling peptide nanofibers containing long motif of laminin influence neurogenesis in in-vitro and in-vivo. *Mol. Neurobiol.* **54**, 1–14 (2016).
20. Wang, L., Xia, J., Li, J., Hagemann, T. L. & Feany, M. B. Tissue and cellular rigidity and mechanosensitive signaling activation in Alexander disease. *Nat. Commun.* **9**, 1899 (2018).
21. Placone, A. L. et al. Human astrocytes develop physiological morphology and remain quiescent in a novel 3D matrix. *Biomaterials* **42**, 134–143 (2015).
22. Lau, L. W., Cua, R., Keough, M. B., Haylock-Jacobs, S. & Yong, V. W. Pathophysiology of the brain extracellular matrix: a new target for remyelination. *Nat. Rev. Neurosci.* **14**, 722–729 (2013).
23. Katarzyna, P. & Janmey, P. A. Glial tissue mechanics and mechanosensing by glial cells. *Front. Cell. Neurosci.* **12**, 25 (2018).
24. Wynn, T. A. Cellular and molecular mechanisms of fibrosis. *J. Pathol.* **214**, 199–210 (2010).
25. Stachel, I., Schwarzenbolz, U., Henle, T. & Meyer, M. Cross-linking of type I collagen with microbial transglutaminase: identification of cross-linking sites. *Biomacromolecules* **11**, 698 (2010).
26. Chau, D. Y. S., Collighan, R. J., Verderio, E. A. M., Addy, V. L. & Griffin, M. The cellular response to transglutaminase-cross-linked collagen. *Biomaterials* **26**, 6518–6529 (2005).
27. Dixon, J. E. et al. Combined hydrogels that switch human pluripotent stem cells from self-renewal to differentiation. *Proc. Natl Acad. Sci. USA* **111**, 5580 (2014).
28. East, E. et al. A 3D in vitror model reveals differences in the astrocyte response elicited by potential stem cell therapies for CNS injury. *Regenerative Med.* **8**, 739–746 (2013).
29. East, E., Golding, J. P. & Phillips, J. B. A versatile 3D culture model facilitates monitoring of astrocytes undergoing reactive gliosis. *J. Tissue Eng. Regenerative Med.* **3**, 634–646 (2009).
30. East, E., Golding, J. P. & Phillips, J. B. Engineering an integrated cellular interface in three-dimensional hydrogel cultures permits monitoring of reciprocal astrocyte and neuronal responses. *Tissue Eng. Part C. Methods* **18**, 526–536 (2012).
31. Rocha, D. N., Ferraz-Nogueira, J. P., Barrias, C. C., Relvas, J. B. & Pêgo, A. P. Extracellular environment contribution to astrogliosis-lessons learned from a tissue engineered 3D model of the glial scar. *Front. Cell. Neurosci.* **9**, 377 (2015).
32. Ying, C. et al. The basic helix-loop-helix transcription factor olig2 is critical for reactive astrocyte proliferation after cortical injury. *J. Neurosci.* **28**, 10983 (2008).
33. Holley, J. E., Gveric, D., Newcombe, J., Cuzner, M. L. & Gutowski, N. J. Astrocyte characterization in the multiple sclerosis glial scar. *Neuropathol. Appl. Neurobiol.* **29**, 434–444 (2010).
34. Liddelow, S. A. & Barres, B. A. Not everything is scary about a glial scar. *Nature* **532**, 182 (2016).
35. Brosius Lutz, A. & Barres, B. A. Contrasting the glial response to axon injury in the central and peripheral nervous systems. *Dev. Cell* **28**, 7–17 (2014).
36. Dias, D. O. & Goritz, C. Fibrotic scarring following lesions to the central nervous system. *Matrix Biol.* **68**, 561–570 (2018).
37. Engler, A. J., Sen, S., Sweeney, H. L. & Discher, D. E. Matrix elasticity directs stem cell lineage specification. *Cell* **126**, 677 (2006).
38. Fu, J. et al. Mechanical regulation of cell function with geometrically modulated elastomeric substrates. *Nat. Methods* **7**, 733–736 (2010).
39. Wisdom, K. M. et al. Matrix mechanical plasticity regulates cancer cell migration through confining microenvironments. *Nat. Commun.* **9**, 4144 (2018).
40. Nam, S., Lee, J., Brownfield, D. G. & Chaudhuri, O. Viscoplasticity enables mechanical remodeling of matrix by cells. *Biophysical J.* **111**, 2296–2308 (2016).
41. Aragona, M. et al. A mechanical checkpoint controls multicellular growth through YAP/TAZ regulation by actin-processing factors. *Cell* **154**, 1047–1059 (2013).
42. Huang, Z. et al. YAP is a critical inducer of SOCS3, preventing reactive astrogliosis. *Cereb. Cortex* **26**, 2299–2310 (2016).
43. Lian, I. et al. The role of YAP transcription coactivator in regulating stem cell self-renewal and differentiation. *Genes Dev.* **24**, 1106–1118 (2010).
44. Yao, F. et al. SKP2- and OTUD1-regulated non-proteolytic ubiquitination of YAP promotes YAP nuclear localization and activity. *Nat. Commun.* **9**, 2269 (2018).
45. Jian, L. T. et al. Cellular mechanosensing of the biophysical microenvironment: a review of mathematical models of biophysical regulation of cell responses. *Phys. Life Rev.* **22–23**, 88–119 (2017).
46. Cheng, B. et al. An integrated stochastic model of matrix-stiffness-dependent filopodial dynamics. *Biophys. J.* **111**, 2051–2061 (2016).
47. Dupont, S. et al. Role of YAP/TAZ in mechanotransduction. *Nature* **474**, 179–183 (2011).
48. Hopkins, A. M., Desimone, E., Chwalek, K. & Kaplan, D. L. 3D in vitro modeling of the central nervous system. *Prog. Neurobiol.* **125**, 1–25 (2015).
49. Burda, J. E. & Sofroniew, M. V. Reactive gliosis and the multicellular response to CNS damage and disease. *Neuron* **81**, 229–248 (2014).
50. Tang-Schomer, M. D. et al. Bioengineered functional brain-like cortical tissue. *Proc. Natl Acad. Sci. USA* **111**, 13811–13816 (2014).
51. Ahmad, A. A. et al. Astrocytes and pericytes differentially modulate blood-brain barrier characteristics during development and hypoxic insult. *J. Cereb. Blood Flow Metab.* **31**, 693–705 (2011).
52. Bercu, M. M. et al. Enhanced survival and neurite network formation of human umbilical cord blood neuronal progenitors in three-dimensional collagen constructs. *J. Mol. Neuroence* **51**, 249–261 (2013).
53. Van Drunen, R. et al. Collagen based multicomponent interpenetrating networks as promising scaffolds for 3D culture of human neural stem cells, human astrocytes, and human microglia. *Acs Applied Bio Materials* **2**, 975–980 (2019).
54. Nakaji-Hirabayashi, T., Kato, K. & Iwata, H. Improvement of neural stem cell survival in collagen hydrogels by incorporating laminin-derived cell adhesive polypeptides. *Bioconjug. Chem.* **23**, 212–221 (2012).
55. Thompson, R. E. et al. Effect of hyaluronic acid hydrogels containing astrocyte-derived extracellular matrix and/or V2a interneurons on histologic outcomes following spinal cord injury. *Biomaterials* **162**, 208–223 (2018).
56. Jimenez-Vergara, A. C., Drunen, R. V., Cagle, T. & Munoz-Pinto, D. J. Modeling the effects of hyaluronic acid degradation on the regulation of human astrocyte phenotype using multicomponent interpenetrating polymer networks (mIPNs). *Sci. Rep.* **10**, 20734 (2020).
57. Neurotoxic reactive astrocytes are induced by activated microglia. *Nature* **541** 481–487 (2017).
58. Pil, Y. S. et al. Block of A1 astrocyte conversion by microglia is neuroprotective in models of Parkinson's disease. *Nat. Med.* **24**, 931–938 (2018).
59. Clark, D. P. Q. et al. Inflammation in traumatic brain injury: roles for toxic A1 astrocytes and microglial–astrocytic crosstalk. *Neurochem. Res.* **44**, 1410–1424 (2019).
60. Hinkle, J. T., Dawson, V. L. & Dawson, T. M. The A1 astrocyte paradigm: new avenues for pharmacological intervention in neurodegeneration. *Mov. Disord.* **34**, 959–969 (2019).
61. Li, T., Chen, X., Zhang, C., Zhang, Y. & Yao, W. An update on reactive astrocytes in chronic pain. *J. Neuroinflammation* **16**, 140 (2019).
62. Li, T., Liu, T., Chen, X., Li, L. & Yao, W. Microglia induce the transformation of A1/A2 reactive astrocytes via the CXCR7/PI3K/Akt pathway in chronic post-surgical pain. *J. Neuroinflammation* **17**, 211 (2020).
63. Atsushi, F. et al. Connexin 30 deficiency attenuates A2 astrocyte responses and induces severe neurodegeneration in a 1-methyl-4-phenyl-1,2,3, 6-tetrahydropyridine hydrochloride Parkinson's disease animal model. *J. Neuroinflammation* **15**, 227 (2018).
64. Basu, A., Krady, J. K. & Levison, S. W. Interleukin-1: a master regulator of neuroinflammation. *J. Neurosci. Res.* **78**, 151–156 (2010).
65. Gold, M. & Khoury, J. E. β-amyloid, microglia, and the inflammasome in Alzheimer's disease. *Semin. Immunopathol.* **37**, 607–611 (2015).

66. Twinkle, C., Matthew, A., Trista, T., Yan, H. & Sandra, H. Interleukin-1β protects neurons against oxidant-induced injury via the promotion of astrocyte glutathione production. *Antioxidants* **7**, 100 (2018).
67. Weinberg, R. P. et al. Palm fruit bioactives modulate human astrocyte activity in vitro altering the cytokine secretome reducing levels of TNFα, RANTES and IP-10. *Sci. Rep.* **8**, 16423 (2018).
68. Goetzl, E. J., Schwartz, J. B., Abner, E. L., Jicha, G. A. & Kapogiannis, D. High complement levels in astrocyte-derived exosomes of Alzheimer's disease. *Ann. Neurol.* **83**, 544–552 (2018).
69. Das, R. K., Gocheva, V., Hammink, R., Zouani, O. F. & Rowan, A. E. Stress-stiffening-mediated stem-cell commitment switch in soft responsive hydrogels. *Nat. Mater.* **15**, 318–25 (2016).
70. Kosako, H. et al. Phosphorylation of glial fibrillary acidic protein at the same sites by cleavage furrow kinase and Rho-associated kinase. *J. Biol. Chem.* **272**, 10333–10336 (1997).
71. Goto, H. et al. Phosphorylation of vimentin by Rho-associated kinase at a unique amino-terminal site that is specifically phosphorylated during cytokinesis. *J. Biol. Chem.* **273**, 11728–11736 (1998).
72. Guasch, R. et al. RhoA and lysophosphatidic acid are involved in the actin cytoskeleton reorganization of astrocytes exposed to ethanol. *J. Neurosci. Res.* **72**, 487–502 (2003).
73. Sun, M., Spill, F. & Zaman, M. H. A computational model of YAP/TAZ mechanosensing. *Biophys. J.* **110**, 2540–2550 (2016).
74. Wan, W. et al. Synergistic effect of matrix stiffness and inflammatory factors on osteogenic differentiation of MSC. *Biophys. J.* **117**, 129–142 (2019).
75. Bangasser, B. L., Rosenfeld, S. S. & Odde, D. J. Determinants of maximal force transmission in a motor-clutch model of cell traction in a compliant microenvironment. *Biophysical J.* **105**, 581–592 (2013).